

Growth, Structure, and Electrophysical Properties of Single Crystals of A_2TiGeO_5 ($A = Li$ and Na)

V. V. Kireev^{1,2}, O. V. Yakubovich³, A. K. Ivanov-Shits¹, O. K. Mel'nikov^{1†},
L. N. Dem'yanets¹, J. Skunman⁴, and N. G. Chaban²

¹Shubnikov Institute of Crystallography, Russian Academy of Sciences, Leninskii pr. 59, Moscow, 117333 Russia

²Lomonosov State Academy of Fine Chemical Technology, pr. Vernadskogo 86, Moscow, 117571 Russia

³Moscow State University, Vorob'evy gory, Moscow, 119899 Russia

⁴Delft Technological University, the Netherlands

Received June 8, 2000

Abstract—Crystals of Li_2TiGeO_5 were obtained by solution-melt crystallization, and those of Na_2TiGeO_5 were grown from a melt by pulling. The crystals are isostructural with the natisite mineral Na_2TiSiO_5 . The crystal structure of $Li_2\{TiOGeO_4\}$ was refined by X-ray diffraction analysis (a four-circle diffractometer, $2\theta/\theta$ scan mode, MoK_α radiation, $\theta_{max} = 50^\circ$). The unit cell parameters are $a = 6.614(4)$ Å and $c = 4.435(4)$ Å; space group $P4/nmm$, $Z = 2$, $\rho_{calcd} = 3.67$ g/cm³, $R = 0.031$, $s = 1.128$, $wR(F^2) = 0.071$ (548 reflections with $I \geq 2\sigma(I)$). The ionic conduction in both crystals was found to be anisotropic in the temperature range 250–600°C. At 400°C, the conductivity values are 10^{-4} to 10^{-5} S/cm along the a axis and 10^{-6} to 10^{-8} (for Na_2TiGeO_5) and 10^{-7} to 10^{-9} S/cm (for Li_2TiGeO_5) along the c axis.

Studying ion transport in solid electrolytes is extremely important as materials of this kind are used in the production of storage cells, batteries, fuel cells, sensors, ion-selective membranes, etc. In the great majority of relevant papers, ionic conduction was studied in polycrystalline samples; however, the specific features of ion transport (including those accounted for by crystal anisotropy) can only be revealed and the grain boundary effect avoided when single crystal parameters are studied.

The crystals of natisite, Na_2TiSiO_5 , and analogous compounds [1–3] with the general formula A_2TiMO_5 (where $A = Li$ or Na and $M = Si$ or Ge) have a pronounced layered structure, in which the main layers of Ti semioctahedra and M tetrahedra alternate with interlayers of mobile cations of alkali metals. As a result, their ionic conduction and other physical properties should be expected to be highly anisotropic.

A synthetic analog of natisite Na_2TiSiO_5 (space group $P4/nmm$) can be obtained only through the hydrothermal method [1–3]. There are two other varieties of this compound. Low-temperature phase crystals (space group $Pmc2_1$) are synthetic analogs of paranatisite [4–6] and can be grown by solution-melt crystallization; when heated to 772°C, these crystals undergo reversible transformation into a high-temperature phase. Insofar as the high-temperature phase cannot be quenched to room temperature, it has not been

adequately studied to date, yet its crystals are known to have tetragonal symmetry.

Compounds Na_2TiGeO_5 [7–9] and Li_2TiSiO_5 [10] exist in only one polymorphous form, which is isostructural with natisite. Their single crystals were obtained by hydrothermal (for the Na analog [7–9]) and solution-melt methods (for the Li analog [10]). Finely crystalline Li_2TiGeO_5 admixed with titanium oxide and lithium germanate was also prepared in [11]. Its structure was studied by the Ritveld method, electron diffraction, NMR spectroscopy, and electron energy loss spectroscopy [11]. Based on the good agreement between the experimental X-ray pattern and that calculated on the assumption that Li_2TiGeO_5 and natisite have the same crystal structure, as well as on the data obtained using direct spectral methods, the authors of [11] inferred that the structure included titanyl groups and a bridging oxygen atom (the Ti–O–Ge bond). However, refined atomic coordinates and thermal parameters for the crystal structure of this phase were absent from their work, which motivated us to carry out a comprehensive X-ray diffraction analysis of the aforementioned structure.

Natisite-like structures were also detected in other materials, e.g., in Li_2VSiO_5 with V^{4+} cations occupying the Ti^{4+} positions [12]. As far as we know, the ionic conduction of the materials under discussion has not been studied to date.

This work was devoted to the growing of massive single crystals of Na_2TiGeO_5 and Li_2TiGeO_5 and to the study of their ionic conduction. Lithium titanoger-

† Deceased.

Table 1. Summary of crystal data, intensity measurement, and structure refinement $\text{Li}_2\text{TiGeO}_5$

Parameter	Value
Formula	$\text{Li}_2\text{TiOGeO}_4$
Absorption μ , mm^{-1}	9.70
Space group	$P4/nmm$
Number of formula units, Z	2
Unit cell parameters, Å	
a	6.614(4)
c	4.435(4)
Density ρ , g/cm^3	3.67
Diffractometer	SYNTEX $P\bar{1}$
Radiation	$\text{MoK}\alpha$ (graphite monochromator)
Temperature (K)	295
Scan range: $2\theta_{\text{max}}$, deg	100.00
Reflection index range	$0 \leq h \leq 10$, $0 \leq k \leq 14$, $0 \leq l \leq 9$
Total number of reflections	550
Number of reflections: independent/observed with $I > 1.96\sigma(I)$	550/548
Refinement	On F^2
Number of refined parameters	20
Absorption correction T_{max} , T_{min}	DIFABS 1.000, 0.284
Discrepancy factors:	
R (for observed reflections)	0.031
wR_2 (for all independent reflections)	0.071
s	1.128

Table 2. Coordinates and equivalent thermal parameters of basic atoms in the structure $\text{Li}_2\text{TiGeO}_5$

Atom	x/a	y/b	z/c	U_{eq} , Å ²
Ti	0.25	0.25	0.1086(1)	0.00292(8)
Ge	0.25	0.75	0.0	0.00247(7)
Li	0.5	0.0	0.5	0.0203(14)
O(1)	0.25	-0.0365(1)	0.2328(2)	0.0055(1)
O(2)	0.25	0.25	0.7264(6)	0.0153(4)

manate was also structurally characterized by X-ray analysis.

EXPERIMENTAL

Growing crystals. Prior to choosing the optimum method of growing the crystals, the behavior of materi-

als in melting was studied by DTA on a Sinku-Riko TGD 7000 derivatograph. Ceramic samples were heated and cooled in a platinum crucible at a rate of 8 K/min. Aluminum oxide was used as the standard.

The starting mixture for growing the crystals of $\text{Li}_2\text{TiGeO}_5$ and $\text{Na}_2\text{TiGeO}_5$ was prepared from Li_2CO_3 , Na_2CO_3 (both reagent grade), TiO_2 , and GeO_2 (both special purity grade). These reagents were mixed in stoichiometric amounts, ground together in an agate mortar, and sintered in two steps. $\text{Li}_2\text{TiGeO}_5$ was initially sintered at 800°C for 12 h, then ground. Then, sintering was continued at 970°C for 6 h. The synthesis of the Na analog was carried out at 730°C for 12 h with subsequent sintering at 810°C for 12 h.

The crystals of $\text{Na}_2\text{TiGeO}_5$ were grown from a melt by pulling (the Czochralski method) at 840–855°C at a rotating rate of 12 rpm. Samples were melted in a platinum crucible 40 ml in volume. Primary crystallization was carried out on a platinum rod 3 mm in diameter; the resulting crystals were used as seeds in subsequent experiments. The pulling rate was varied from 0.5 to 2.0 mm/h; the best crystals were obtained at a rate of 0.5 mm/h.

The crystals of $\text{Li}_2\text{TiGeO}_5$ were grown by the solution-melt method. A mixture of Li_2MoO_4 (80 wt %) and Li_2WO_4 (20 wt %) was used as a solvent. The $\text{Li}_2\text{TiGeO}_5$ mixture and the solvent were taken in the ratio 6 : 5 (by weight). The reagents were melted in a hemispherical platinum bowl 48 mm in diameter. Crystallization was carried out on a platinum rod 3 mm in diameter. The starting mixture was heated in the solvent at 1030°C until complete dissolution and then cooled to 980°C at a rate of 10 K/h; crystallization occurred upon cooling from 968 to 958°C at a rate of 0.05 K/h. Because lithium molybdate and lithium tungstate are water soluble, they were removed by washing the obtained crystals with water at room temperature for 12 h.

The conversion completeness in the synthesis of $\text{Li}_2\text{TiGeO}_5$ and $\text{Na}_2\text{TiGeO}_5$ was checked, and phase identification was performed by X-ray diffraction analysis (a Rigaku D maxIIIc diffractometer, $5^\circ < 2\theta < 80^\circ$, $\text{CuK}\alpha_1$ radiation ($\lambda = 1.05456$ Å)). Prior to recording X-ray patterns, test samples were ground in an agate mortar.

The optical absorption spectra of the crystals were recorded on a Varian spectrometer in the range 200–900 nm.

X-ray diffraction analysis. To refine the crystal structure of $\text{Na}_2\text{TiGeO}_5$ [8], the crystals obtained by hydrothermal synthesis were used. The unit cell parameters for $\text{Li}_2\text{TiGeO}_5$ were refined in the study of a tabular crystal ($0.3 \times 0.3 \times 0.1$ mm) on a Syntex P1 four-circle diffractometer. A summary of the crystal data, intensity measurement, and structure refinement for $\text{Li}_2\text{TiOGeO}_4$ is given in Table 1.

All calculations were performed with the SHELXL program [13]. Atomic scattering curves and corrections for anomalous dispersion were borrowed from [14].

The structure was refined in the full-matrix anisotropic approximation. The final residual was $R = 0.031$. The coordinates and equivalent thermal parameters of the basic atoms are listed in Table 2.

Study of conduction. The samples used for the conduction study were rectangular parallelepipeds with edges parallel to the specific directions in the tetragonal cell units of the $\text{Na}_2\text{TiGeO}_5$ and $\text{Li}_2\text{TiGePO}_5$ crystals.

Ionic conduction was studied by impedance spectroscopy. To provide for a more reliable treatment of the results obtained, the impedance was measured in each direction for several crystals with different size factors, k ($k = l/S$, where l is the electrode spacing and S is the electrode area).

Frequency characteristics were recorded in an electrochemical cell with silver or platinum electrodes to block the Li^+ and Na^+ ions. The silver electrodes were prepared by applying a paste and its caking at 600°C for 1 h. The platinum electrodes were made by applying platinum in two steps. First, a thin film of platinum was deposited by spraying for 12 min (Edwards Sputter Coater S150B, argon pressure 7 mbar, current 20 mA). Then, the crystals were coated with a platinum paste over the deposited layer, which was allowed to cake at 600°C for 1 h.

The complex impedance of the samples was measured on a Solartron 1260 analyzer in the frequency range 1 Hz to 10 MHz at a potential amplitude 250 mV (the measured response was virtually independent of the signal amplitude in the range 50–250 mV, while the noise-to-signal ratio significantly increased at low voltage). The experiments were carried out in a nitrogen atmosphere at 250 to 600°C (below 250°C , the impedance of the samples became comparable to the analyzer's output resistance). The impedance spectra were processed using the EQUIVCRT program [15].

RESULTS AND DISCUSSION

Crystal characterization. The thermograms of $\text{Na}_2\text{TiGeO}_5$ and $\text{Li}_2\text{TiGeO}_5$ ceramics are shown in Fig. 1. Sodium titanogermanate experiences no phase transitions in the range from room temperature to its melting point at 910°C . The presence of a single peak at 845°C in the cooling curve suggests a melting of congruent character. The resulting sample (after melting and crystallization) was found to be identical to the starting sample (X-ray phase analysis).

Lithium titanogermanate shows no phase transitions in the range from room temperature to its melting point at 1180°C , but its cooling curve exhibits several peaks. According to X-ray phase data, the products subjected to melting and crystallization do not contain the starting material. The X-ray pattern of the solidified melt shows, along with the peaks corresponding to Li_2GeO_3 and products of partial reduction of titanium dioxide (TiO , Ti_4O_7 , and Ti_3O_5), additional, unidentified peaks. Therefore, this melt is a multicomponent mixture and

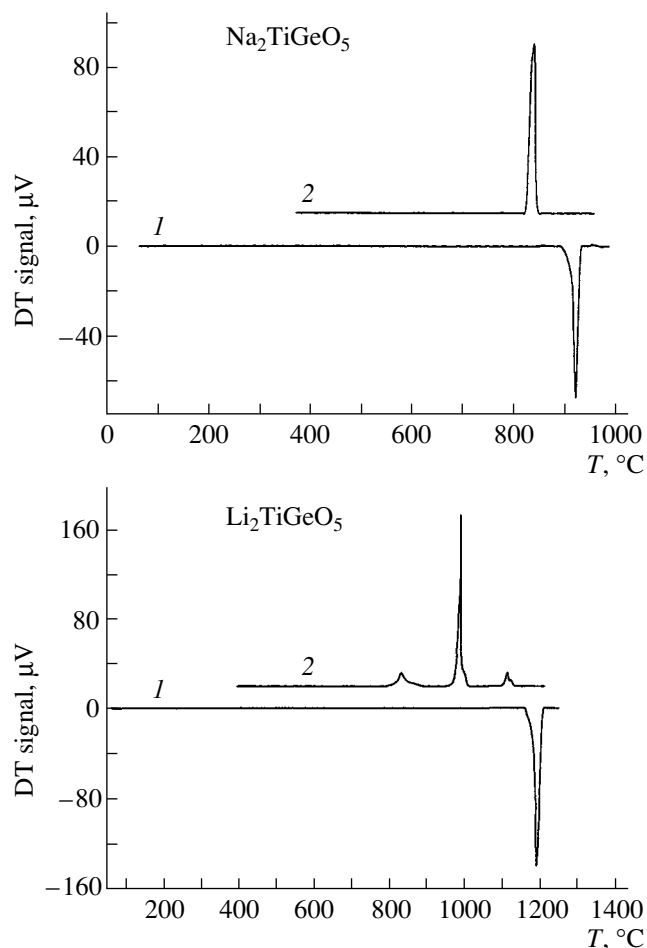


Fig. 1. Thermograms of $\text{Na}_2\text{TiGeO}_5$ and $\text{Li}_2\text{TiGeO}_5$ ceramics: (1) heating and (2) cooling.

lithium titanogermanate melts in an incongruent way. Its crystals, unlike those of $\text{Na}_2\text{TiGeO}_5$, cannot be grown from a melt. Our attempts at growing crystals of sodium titanogermanate by the hydrothermal method for ionic conduction study [8] failed, because the resulting crystals were too small and unsuitable for electrophysical measurements. In this work, the crystals of $\text{Na}_2\text{TiGeO}_5$ and $\text{Li}_2\text{TiGeO}_5$ were grown from a melt by pulling and crystallized from a solution in a melt, respectively.

The crystals of $\text{Na}_2\text{TiGeO}_5$ were obtained as pellets of crystal aggregations 25 mm long and 5 to 7 mm in diameter. Because of their perfect cleavage perpendicular to the c axis, the crystals can be split (while sawing a pellet with a circular saw) into separate single-crystal plates no greater than $2 \times 5 \times 6$ mm or into aggregations composed of two to three crystals. The resulting colorless plates are visually transparent along the c axis. The near UV–VIS absorption spectrum of $\text{Na}_2\text{TiGeO}_5$ (Fig. 2) contains a sharp peak at 270 nm in the near UV region and no peaks in the visible range (absorption is independent of the wavelength), for which reason the crystals are colorless. Cleavage along the a axis is very

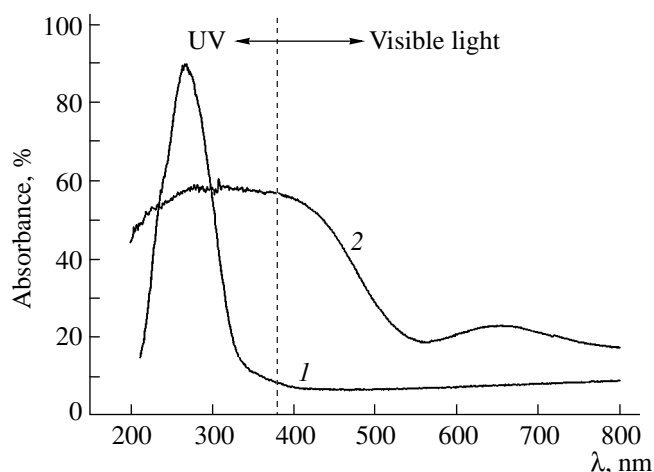


Fig. 2. UV–VIS absorption spectra of the crystals of (1) $\text{Na}_2\text{TiGeO}_5$ and (2) $\text{Li}_2\text{TiGeO}_5$.

poor. The fracture perpendicular to this direction is opaque and, when examined under microscope, shows surface imperfections and layers perpendicular to the c axis. Along these layers (i.e., perpendicular to the c axis), the crystal is eutomous and can be easily split with a razor blade.

The $\text{Li}_2\text{TiGeO}_5$ phase was obtained as hemispherical nodules (crystal aggregations). Separate crystal plates are clearly discernible on the nodule surface and can be easily split along the cleavage planes with a razor blade. The cleavage of lithium titanogermanate is perfect along the c axis and less perfect along the a axis, being more distinct in both directions than that of $\text{Na}_2\text{TiGeO}_5$. $\text{Li}_2\text{TiGeO}_5$ forms yellow–green transparent, tabular crystals. Its near UV–VIS absorption spectrum is displayed in Fig. 2. The yellow–green color of the crystals is due to the minimum absorption at 650 nm. The absorption peak in the near UV region is diffuse and overlaps the visible range, as distinct from the analogous peak for $\text{Na}_2\text{TiGeO}_5$. The coloration of the $\text{Li}_2\text{TiGeO}_5$ crystals is due to impurities of, most likely, Mo and W passed to the crystal from the melt. The plate size is no larger than $1.2 \times 18 \times 6$ mm. Because of cleavage, the fracture perpendicular to the a axis is even and transparent. Microscopic examination reveals lamination along the c axis.

X-ray powder patterns of the crystals (Table 3) and ceramic samples proved to be the same for each crystal–ceramic pair, indicating that the crystalline phases obtained by solid-state synthesis are identical to the grown crystals. In addition, according to X-ray phase data, our Czochralski grown single crystals of $\text{Na}_2\text{TiGeO}_5$ are identical to those obtained earlier by the hydrothermal method [8].

Crystal structure. In the structure $\text{Li}_2\text{TiOGeO}_4$ (Fig. 3), the coordination polyhedron of Ti is a semioc-tahedron (or tetragonal pyramid) with symmetry D_{4v} . According to this symmetry, four oxygen atoms are

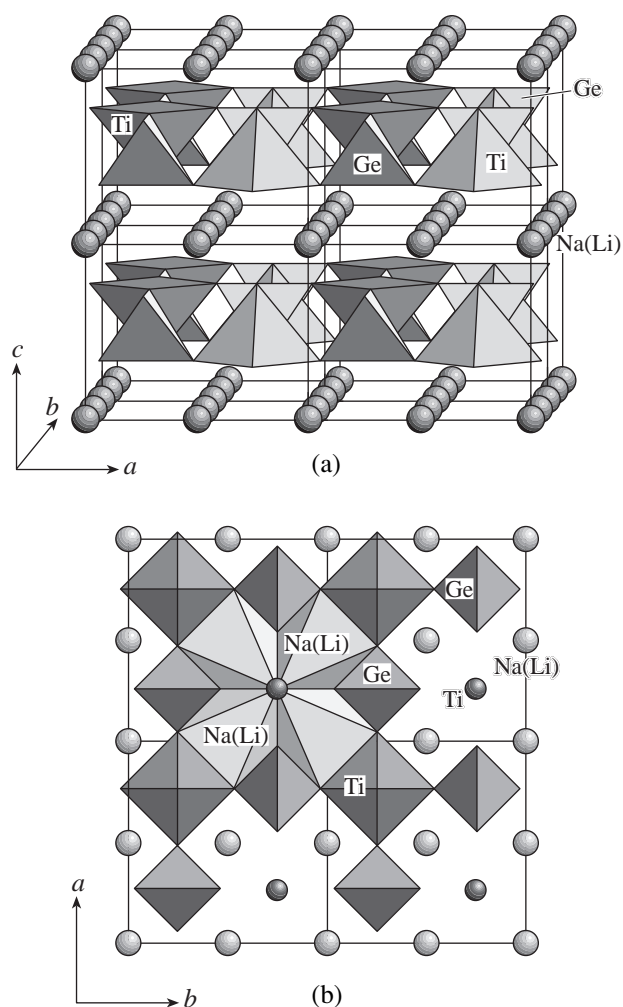


Fig. 3. Crystal structure of A_2TiGeO_5 ($\text{A} = \text{Na}$ and Li) in (a) axonometric projection and (b) projection onto the ab plane.

equidistant (Ti–O(1) 1.973(1) Å), while the distance from the fifth, apical oxygen atom is shorter (Ti–O(2) 1.695(3) Å). Analogous distances in an isostructural synthetic silicate, $\text{Li}_2\text{TiOSiO}_4$, are equal to 1.967(1) and 1.698(3) Å, respectively [10]. For isotypical Na analogs, the corresponding Ti–O bond lengths equal 1.990(2) and 1.695(5) Å in $\text{Na}_2\text{TiOSiO}_4$ [2] and 1.993(2) and 1.708(5) Å in $\text{Na}_2\text{TiOGeO}_4$ [8]. The interatomic cation–oxygen distances in the VO_5 pyramid of the $\text{Li}_2\text{VOSiO}_4$ structure is naturally shorter (1.955(3) Å for the pyramid base and 1.623(6) Å for the vertex) [12]. In the latter case, the vanadyl group is fixed even stronger than the titanyl group in the titanium-containing phases of this structural type.

In near-regular GeO_4 tetrahedra of $\text{Li}_2\text{TiOGeO}_4$, the Ge–O bond lengths are equal to 1.749(1) Å. The Li–O(1) ($\times 4$) and Li–O(2) ($\times 2$) distances in centrosymmetric LiO_6 octahedra (symmetry C_{2h}) are 2.049(1) and 2.545(2) Å, respectively.

The crystals of $\text{Li}_2\text{TiGeO}_5$ and $\text{Na}_2\text{TiGeO}_5$ contain mixed-type anionic $\{\text{TiO}[\text{SiO}_4]\}_\infty$ layers—topologically identical to $\{\text{TiO}[\text{GeO}_4]\}_\infty$ layers in natisite—composed of TiO_5 semi-octahedra and GeO_4 tetrahedra sharing the oxygen vertices and staggered in the ab plane. Along the c axis of the unit cell, these layers alternate with layers of Li^+ and Na^+ cations in distorted tetrahedra with shared edges (Fig. 3).

The geometric parameters of tetragonal unit cells of Ti-containing natisite-like phases and interatomic cation–oxygen distances in the main building blocks (octahedra, semi-octahedra, and tetrahedra) of their crystals are given in Table 4. When comparing the chemical formulas of four compounds with their unit cell parameters, one can easily see that parameter $a(b)$ is primarily determined by the size of the cation in the tetrahedral position. Thus, these values in Ge phases are naturally higher than those in Si analogs. By contrast, the increase in parameter c for Na-containing phases is associated with the size of the univalent cation in the interlayer area.

At first glance, it is not obvious why TiO_5 semi-octahedra—an essential part of all of the four crystal structures—are significantly more distorted in Na analogs. The character of the crystal structure implies that an anionic $\{\text{TiOGeO}_4\}_\infty^{2-}$ layer and a cationic layer composed of AO_6 octahedra ($A = \text{Na}$ or Li) share the edges of the TiO_5 semi-octahedra and the univalent Na^+ or Li^+ octahedra. Each TiO_5 semi-octahedron shares four basic edges with four AO_6 octahedra ($A = \text{Na}$ or Li) in the neighboring layer (along the c axis), in which the corresponding four edges of each octahedron are shared with like neighbors (Fig. 3b). In this case, the structural fragments should fit into one another to form a rigid construction; as a result, the polyhedra become distorted. Because Ti^{4+} and Li^+ cations have close ion radii, their edge contacts are possible for a relatively low anisotropy of Ti–O bonds in a semi-octahedron. This is due, in this case, only to the specific electron shell of the titanium atom.

Another reason for the more considerable distortion of the TiO_5 semi-octahedra in Na-containing phases is that the shared edges of the polyhedra of the Na^+ and Ti^{4+} cations, whose radii differ greatly, must also match in length. It is interesting that bond anisotropy in the cationic layer of lithium natisites is higher than that in sodium analogs (interatomic Li–O(2) distances from the apical octahedral vertices are much longer than the other four Li–O(1) bonds). This is due to the multiplicity factors, dictated by anionic $\{\text{TiOGeO}_4\}_\infty^{2-}$ or $\{\text{TiOSiO}_4\}_\infty^{2-}$ layers, of the unit cells along the x and y axes having to be kept constant.

Ionic conduction. The complex impedance of the $\text{Na}_2\text{TiGeO}_5$ crystals, measured along the a and c axes, and the equivalent circuit diagrams are shown in Fig. 4.

Table 3. X-ray patterns for $\text{Na}_2\text{TiGeO}_5$ and $\text{Li}_2\text{TiGeO}_5$ (plane spacing, intensities, and reflection indices)

$\text{Na}_2\text{TiGeO}_5$			$\text{Li}_2\text{TiGeO}_5$		
$d, \text{Å}$	I/I_0	hkl	$d, \text{Å}$	I/I_0	hkl
5.139	66	0 0 1	4.667	6	1 1 0
4.672	2	1 1 0	4.423	100	0 0 1
4.051	12	0 1 1	3.675	29	0 1 1
3.461	8	1 1 1	3.302	65	0 2 0
3.312	23	0 2 0	3.215	15	1 1 1
2.784	100	0 2 1	2.648	70	0 2 1
2.567	14	1 2 1	2.457	5	1 2 1
2.395	11	0 1 2	2.339	8	2 2 0
2.345	13	2 2 0	2.098	11	0 1 2
2.253	6	1 1 2	2.065	13	2 2 1
2.134	2	2 2 1	2.001	10	1 1 2
2.032	6	3 0 1	1.973	8	0 3 1
1.941	2	3 1 1	1.892	4	3 1 1
1.733	23	3 2 1	1.839	6	0 2 2
1.678	3	0 3 2	1.774	6	1 2 2
1.659	15	0 4 0	1.653	13	4 0 0
1.626	6	1 3 2	1.608	12	2 2 2
1.611	2	4 1 0	1.549	6	0 4 1
1.578	3	4 0 1	1.520	9	3 1 2
1.523	10	0 2 3	1.479	6	2 4 0
1.485	8	2 4 0	1.402	10	4 2 1
1.427	12	2 4 1	1.321	5	1 2 3
1.395	3	0 4 2	1.298	2	1 5 0
1.385	2	2 2 3	1.274	3	3 3 2
1.337	1	3 3 2	1.229	2	2 5 0
1.328	3	3 4 0	1.206	4	3 1 3
1.286	3	5 0 1			
1.241	2	1 1 4			

Table 4. Geometric parameters of the synthetic natisite-like phases

Parameter, Å	$\text{Na}_2\text{TiOGeO}_4$	$\text{Na}_2\text{TiOSiO}_4$	$\text{Li}_2\text{TiOGeO}_4$	$\text{Li}_2\text{TiOSiO}_4$
a	6.658	6.480	6.614	6.438
c	5.161	5.107	4.435	4.400
Ti–O(1)	1.993	1.990	1.973	1.967
Ti–O(2)	1.708	1.695	1.695	1.698
Ge–O	1.748		1.749	
Si–O		1.636		1.633
Na–O(1)	2.307	2.307		
Li–O(1)			2.049	2.057
Na–O(2)	2.669	2.584		
Li–O(2)			2.545	2.460

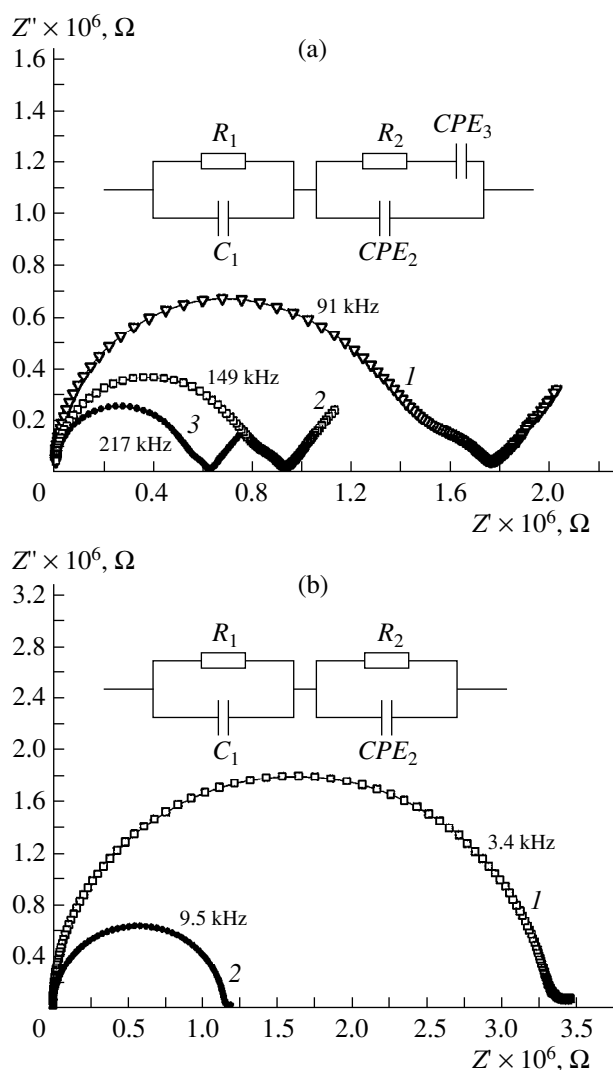


Fig. 4. Frequency dependences of the complex impedance of $\text{Na}_2\text{TiGeO}_5$ crystals and equivalent circuits for (a) a Pt electrode and the crystal oriented along the a axis at (1) 335, (2) 375, and (3) 402°C and (b) an Ag electrode and the crystal oriented along the c axis at (1) 508 and (2) 538°C.

Similar diagrams were obtained for lithium crystal. The shape of the impedance locus is independent of whether a silver or platinum electrode is used in the electrochemical cell, but differs for samples oriented along the a and c axes. In the former case, the impedance locus consists of a high-frequency semicircle, a distorted medium-frequency semicircle, and a low-frequency straight line, the semicircles partially overlapping. Mathematical processing showed that the frequency dependence of the crystal impedance along the c axis consists of two superimposed semicircles. The R_1C_1 and R_2CPE_2 circuits (CPE means “constant phase element”) in the equivalent circuit diagrams correspond to the high- and medium-frequency semicircles, respectively; the CPE_3 element corresponds to the low-frequency straight line.

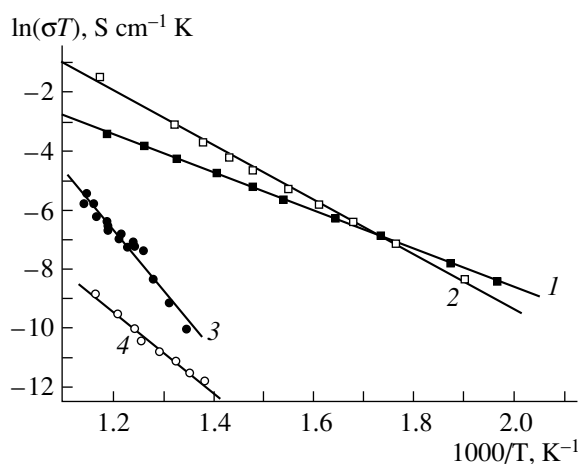


Fig. 5. Temperature dependences of the bulk conductivity of (1, 3) $\text{Na}_2\text{TiGeO}_5$ and (2, 4) $\text{Li}_2\text{TiGeO}_5$ for crystals oriented along (1, 2) the a axis and (3, 4) the c axis. $E_a =$ (1) 0.55, (2) 0.80, (3) 1.78, and (4) 1.18 eV.

To interpret the elements of the equivalent circuit, we measured the impedance of the crystals for different size factors and electrodes (Ag and Pt). A detailed report on these studies will be published at a later date (In Solid State Ionics Journal). In most cases, the conductivity calculated from R_1 is independent of the size factor and the electrode material, as distinct from that based on R_2 . C_1 is always close to the capacitance of a disconnected cell. Thus, R_1 is the bulk impedance of a crystal, C_1 is the geometric capacitance of a cell, and R_2 , CPE_2 , and CPE_3 are related to various relaxation processes (diffusion of charge carriers, effect of surface roughness, polarization, and electrode–electrolyte interaction) and were not examined extensively in this work.

Temperature vs. bulk conductivity curves for differently oriented crystals of $\text{Na}_2\text{TiGeO}_5$ and $\text{Li}_2\text{TiGeO}_5$ in cells with platinum electrodes are shown in Fig. 5. These data were used to calculate corresponding activation energies. As can be seen in Fig. 5, both crystals are characterized by high conduction anisotropy $(\sigma \parallel a)/(\sigma \parallel c) = 10^2$ to 10^3 for $\text{Na}_2\text{TiGeO}_5$ and 10^3 to 10^4 for $\text{Li}_2\text{TiGeO}_5$.

It is noteworthy that the conductivity of $\text{Na}_2\text{TiGeO}_5$ along the c axis is much higher than the analogous value for $\text{Li}_2\text{TiGeO}_5$. The specific features of crystal structure (Fig. 3) make conduction in this direction impossible in a perfect crystal. If one assumes that the conduction along the c axis occurs via linear or three-dimensional defects, the concentration of such defects in $\text{Na}_2\text{TiGeO}_5$ should be higher than that in $\text{Li}_2\text{TiGeO}_5$.

While analyzing the possibility of cationic conduction along the a axis, note that, in both of the materials under discussion, all octahedral sites in the cationic layers are occupied by alkali metal atoms, suggesting that there are no prerequisites for cation transport in a per-

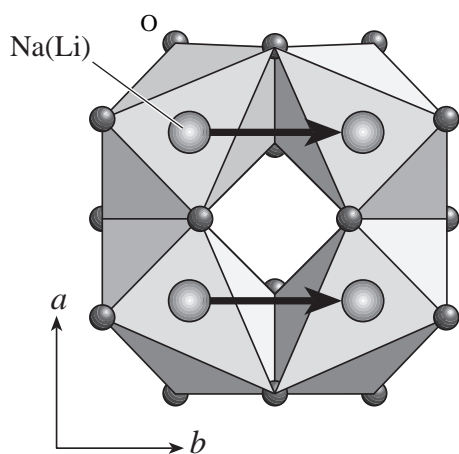


Fig. 6. Coordination polyhedra and the ways of migration of the alkali metal cations in structures A_2TiGeO_5 ($A = Na(Li)$).

fect crystal. Migration probably occurs through Na^+ and Li^+ vacancies formed by extrinsic impurities during crystal growth. A small portion of such vacancies can result from the migration of a crystal's own atoms leaving their crystallographic sites (heat defects); they are thus immanent property of the structure. In this case, the number of vacancies is very small and, accordingly, the conductivity is low.

Usually, ion conductors exhibit high conductivity at vacancy concentrations no less than 5 to 10%. This can be reached only when impurities are purposefully added or there is intrinsic structural disorder, which can be detected by modern X-ray diffraction methods. The paths of possible migration of mobile univalent cations in the structures under examination are shown in Fig. 6. Analysis of the interatomic distances and the O^{2-} , Na^+ , and Li^+ ion radii allows one to conclude that the migration of an alkali cation (Fig. 6) displaces oxygen atoms, thus inevitably distorting the conduction channel.

Further investigations into the synthesis of analogous materials with high concentration of alkali cation vacancies are of interest, as they allow highly conducting crystals to be obtained.

ACKNOWLEDGMENT

This work was supported by the Russian Foundation for Basic Research, project nos. 00-05-64312 and 00-15-98582; the RF Ministry of Education, grant no. 97-9.2-33; and the NWO project, grant no. 047-007-008.

REFERENCES

1. Nikitin, A.V., Ilyukhin, V.V., Mel'nikov, O.K., and Belov, N.V., *Dokl. Akad. Nauk SSSR*, 1964, vol. 157, no. 6, p. 1355.
2. Nyman, H., O'Keeffe, M., and Bovin, J.-O., *Acta Crystallogr., Sect. B: Struct. Crystallogr. Cryst. Chem.*, 1978, vol. 34, no. 3, p. 905.
3. Egorov-Tismenko, Yu.K., Simonov, M.A., and Belov, N.V., *Dokl. Akad. Nauk SSSR*, 1978, vol. 240, no. 1, p. 78.
4. Bayer, G., Florke, O.W., Hoffmann, W., and Scheel, H.-J., *Glastech. Ber.*, 1966, vol. 39, no. 5, p. 242.
5. Glasser, F.P. and Marr, J., *J. Am. Ceram. Soc.*, 1979, vol. 62, no. 1, p. 42.
6. Ziadi, A., Hillebrecht, H., Thiele, G., and Elouadi, B., *J. Solid State Chem.*, 1996, vol. 123, p. 324.
7. Verkhovskii, V.Ya., Kuz'min, E.A., Ilyukhin, V.V., and Belov, N.V., *Dokl. Akad. Nauk SSSR*, 1970, vol. 190, no. 1, p. 91.
8. Yakubovich, O.V., Kireev, V.V., and Mel'nikov, O.K., *Kristallografiya*, 2000, vol. 45, no. 4, p. 635.
9. Ilyushin, G.D. and Dem'yanets, L.N., *Itogi Nauki Tekh., Ser.: Kristallokhimiya*, 1989, vol. 22, p. 45.
10. Ziadi, A., Thiele, G., and Elouadi, B. *J. Solid State Chem.*, 1994, vol. 109, p. 112.
11. Bastow, T.J., Botton, G.A., Etheridge, J., *et al.*, *Acta Crystallogr., Sect. A: Found. Crystallogr.*, 1999, vol. 55, no. 2(1), p. 127.
12. Rangan, K.K., Pyffard, Y., Joubert, O., and Tournoux, M., *Acta Crystallogr., Sect. C: Cryst. Struct. Commun.*, 1998, vol. 54, no. 2, p. 176.
13. Sheldrick, G.M., *SHELXL97. Program for the Refinement of Crystal Structures From Diffraction Data*, Univ. of Göttingen, 1997.
14. *International Tables of Crystallography*, Hahn., T., Ed., Dordrecht: D. Riedel, 1995, vol. A.
15. Boukamp, B.A., *Solid State Ionics*, 1986, vol. 20, p. 31.